Catalytic deoxygenation on transition metal carbide catalysts

Journal:	*Catalysis Science & Technology*
Manuscript ID	CY-PER-10-2015-001665.R1
Article Type:	Perspective
Date Submitted by the Author:	16-Dec-2015

Complete List of Authors:	Sullivan, Mark; University of Minnesota, Chemical Engineering and Materials Science Chen, Cha-Jung; University of Minnesota, Chemical Engineering and Materials Science Bhan, Aditya; University of Minnesota, Chemical Engineering and Materials Science

Catalytic deoxygenation on transition metal carbide catalysts

Mark M. Sullivan, Cha-Jung Chen, Aditya Bhan*

Department of Chemical Engineering and Materials Science

University of Minnesota - Twin Cities

421 Washington Avenue SE

Minneapolis, Minnesota 55455

USA

E-mail address: sulli931@umn.edu (M. M. Sullivan), chenx990@umn.edu (C.-J. Chen), and abhan@umn.edu (A. Bhan)

*Corresponding author

Abstract

We discuss the evolution of catalytic function of interstitial transition metal formulations as a result of bulk and surface structure modifications via alteration of synthesis and reaction conditions, specifically, in the context of catalytic deoxygenation reactions. We compare and contrast synthesis techniques of molybdenum and tungsten carbides, including temperature programmed reaction and ultra-high vacuum methods, and note that stoichiometric reactions may occur on phase-pure materials and that in situ surface modification during deoxygenation likely results in the formation of oxycarbides. We surmise that catalytic metal-acid bifunctionality of transition metal carbides can be tuned via oxygen modification due to the inherent oxophilicity of these materials and demonstrate the use of in situ chemical titration methods to assess catalytic site requirements on these formulations.

Table of contents entry:
We highlight the evolution and tunability of catalytic function of transition metal carbides under oxidative environments for selective deoxygenation reactions.

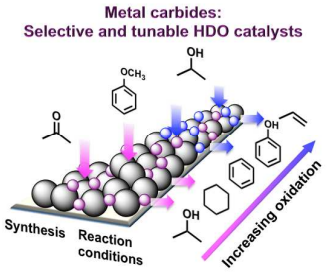

1. Introduction

Transition metal carbides that have been shown to catalyze hydrogenolysis,[1,2] hydrogenation,[2–8] and isomerization[9–12] reactions and to exhibit both metallic and acidic characteristics are now finding applications in electrocatalytic hydrogen evolution (HER)[13–15] and hydrodeoxygenation (HDO) of biomass-derived oxygenates to fuels and chemicals.[16–26] These interstitial compounds[27] display extensive non-uniformities, including distinct binding sites,[28–33] thermodynamically stable surfaces with varying terminations,[34] and non-stoichiometric compositions in the ratios of transition metal, C, and O both in the bulk and surface structures[8,35] (Scheme 1) as evinced by spectroscopic and mechanistic studies of specific reaction systems, ultra-high vacuum surface science studies, and computational calculations. HDO of lignocellulosic or triglyceride-based biomass requires selective cleavage of strong carbon-oxygen bonds (>385 kJ mol^{-1})[36] without successive hydrogenation and/or undesired C-C scission. Severe reaction conditions such as high temperature (~700 K) and high hydrogen pressures (1–10 MPa) are often employed for HDO reactions using noble metal catalysts, resulting in the loss of carbon and/or excess use of hydrogen in concurrent decarboxylation, hydrogenation, and hydrocracking reactions.[36–39] The co-existence of metallic and acidic functionalities on transition metal carbides is attractive for HDO because the presence of oxygen on/in carbides can simultaneously inhibit the metallic function and enhance acidic character,[7,10–12,40] which potentially allows for selective deoxygenation at ambient pressure and low temperatures (420–553 K).

In this perspective, we focus on HDO chemistries over transition metal carbides, specifically, the characteristics that result in selective deoxygenation, and we discuss the tunability and evolution of the catalytic function from monofunctional metallic to bifunctional metallic–acidic to monofunctional acidic in the reaction environment in context of structural/compositional variation in carbidic formulations as a result of synthesis and/or reaction conditions. This work primarily discusses molybdenum carbidic formulations while emphasizing similarities and denoting differences between molybdenum- and tungsten-carbidic catalysts. We highlight the necessity to incorporate transient kinetic studies and in situ chemical titration to probe catalytic sites on transition metal carbides during HDO reactions due to the inherent structural variability of these carbidic catalysts.

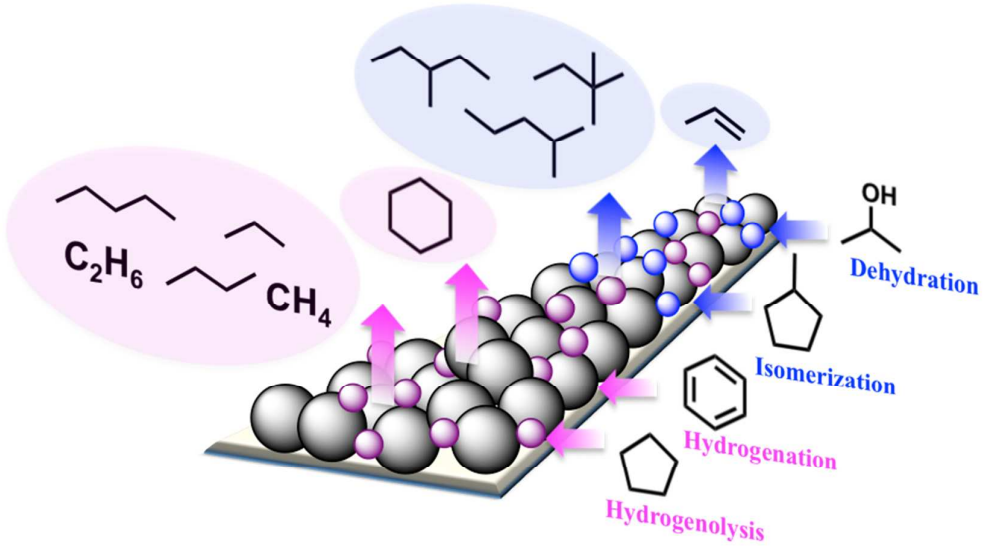

Scheme 1. Catalytic reactions – including hydrogenolysis, hydrogenation, isomerization, and dehydration – that are catalyzed by carbidic and oxycarbidic molybdenum carbide formulations.

2. Structure

Transition metals such as molybdenum alter their structure by lattice expansion and concurrent incorporation of heteroatoms (C, O, N) into interstitial sites, typically the octahedral sites of a face-centered cubic (fcc) or hexagonal close-packed (hcp) lattice, as discussed in the extensive review on this topic by Oyama.[41] Interstitial molybdenum compounds often form distorted, vacancy-dense structures.[42] Metallic molybdenum and tungsten both adopt body-centered cubic (bcc) structures, and both can form analogous carbidic crystal structures.[41] Stable molybdenum oxides such as MoO_3 and MoO_2 exist as layers of edge-sharing distorted MoO_6 octahedra and distorted rutile structures with six-coordinated Mo, respectively. Interstitial carbide structures of varying bulk stoichiometries (MoC_x, x ~0.5 – 1) have been reported.[43] Most commonly reported are the structurally similar orthorhombic Mo_2C and the hexagonally close-packed Mo_2C, nearly indistinguishable using X-ray diffraction (XRD) analysis.[44]

Metastable fcc MoC_{1-x} (x ~0.5) has also been experimentally observed via XRD. Ledoux and co-workers[45] synthesized an fcc oxycarbidic phase ($MoO_{2.42}C_{0.23}H_{0.78}$) that was isostructural to other reported fcc carbides; the synthesis of this phase was attributed to the presence of metal vacancies that promote heteroatom mobility. De Oliveira also reported the thermodynamic stability of abundant vacancies within carbide formulations (~10% for both C and Mo vacancies) based on the implementation of a Helmholtz free energy minimization technique using density functional theory (DFT) optimized structures. These vacancies can facilitate heteroatom and hydrogen diffusion,[46] partially explaining the structural variability of these interstitial formulations.

The surface termination of synthesized interstitial molybdenum formulations also varies. Wang et al.[34] used DFT to demonstrate the thermodynamically favorable surface terminations and crystal structures as a function of the carburizing potential of the synthesis gas environment. By minimizing calculated surface energy, Wang and coworkers investigated the 22 different surface terminations of the 7 low Miller index planes of orthorhombic Mo_2C, demonstrating the large number of thermodynamically favorable surface terminations as a function of reaction or synthesis conditions, specifically noting the favorability of forming mixed Mo/C or C-terminated surfaces with increasing carburizing potential in contrast to forming Mo-terminated surfaces under low carburizing potentials. These reports demonstrate that interstitial molybdenum structures are complex in and of themselves and that the bulk and surface structure of these formulations are a function of synthesis conditions; we discuss below the effects of surface termination on catalytic function.

3. Catalyst synthesis, characterization, and surface science

Sinfelt reported quasi-autocatalytic ethane hydrogenolysis on Mo-based formulations to occur via progressive Mo carburization at 668 K under flowing H_2/C_2H_6.[47] This work elegantly demonstrated the importance of both the surface and bulk crystal structures in relation to catalytic activity, and most importantly how in situ modification of structure and function arises during reaction. Oyama[41] and Chen and co-workers[17,48] extensively reviewed synthesis techniques of transition metal interstitial oxides, carbides, and nitrides as well as their reactivities, demonstrating the importance of reactor studies, DFT, and surface science in probing the effects of structure and surface termination upon reactions catalyzed by

interstitial transition metal catalysts. We focus on recent experimental work investigating transition metal carbide catalytic formulations synthesized via two techniques: (i) in situ temperature programmed reaction (TPR) techniques used primarily in microreactor experimental studies, and (ii) in situ ultra-high vacuum (UHV) synthesis via carburization of Mo or W foils and the use of these formulations for catalytic deoxygenation.

3.1. Synthesis of transition metal carbide formulations via temperature programmed reaction

The synthesis of self-supporting, high surface area (60-100 m^2 g^{-1}) molybdenum carbide catalysts using TPR was developed by Boudart and coworkers.[49] Treating a Mo-oxide precursor under continuous H_2/hydrocarbon flow of differing compositions during varying temperature ramp rates up to 1023 K results in the synthesis of interstitial molybdenum carbide formulations of varying surface and bulk compositions.[7,49] Djéga-Mariadassou and co-workers[7] demonstrated the progressive structural alteration of the oxide precursor during TPR via sequential synthesis, quenching, and X-ray diffraction (Figure 1). The crystal structure of the oxide precursor was noted to transform from molybdic acid to Mo_4O_{11} to MoO_2 to Mo to Mo_2C, and these transformations were noted to involve sequential and occasionally simultaneous loss of lattice oxygen as H_2O and lattice carburization via CH_4. TPR syntheses for WC_x catalysts are conducted under similar H_2/hydrocarbon flow conditions with a tungsten oxide precursor, but final synthesis temperatures are typically higher and can be as high as 1273 K.[23,24]

The structural changes observed are a function of thermodynamic potentials of the carburizing gas and H_2 as discussed by Lee and coworkers (Figure 2) which can alter the deposition of polymeric surface carbon or the over-reduction of the carbide to metallic Mo.[49] Maintenance of a high surface area product is affected by both the thermodynamics and the kinetics of the TPR; avoiding overreduction and bypassing formation of metallic Mo is necessary to overcome the propensity of Mo sintering due to its low Tammann temperature compared to that of the interstitial carbides, oxides, and nitrides.[41] Difficulties in producing phase-pure carbides also arise from inability of the reductive H_2 atmosphere to completely remove oxygen from the Mo-oxide precursor, demonstrated by the inhibitive effect of residual oxygen on benzene hydrogenation observed by Djéga-Mariadassou and coworkers.[7]

Mo_2C syntheses via TPR-induced reductive removal of oxygen produce oxophilic carbide surfaces whose pyrophoric nature necessitates passivation prior to any ex situ characterization. Passivation is typically carried out using dilute O_2 flow at ambient temperature in order to oxidize the carbide surface without affecting the bulk crystal structure.[16,49] Passivated catalysts demonstrate retention of bulk carbide structures as evinced by X-ray diffraction.[7] However, passivation treatments oxidize the carbide surface structure, rendering difficulty in ascertaining the composition of the surface present under reaction conditions using ex situ surface characterization methods such as X-ray photoelectron spectroscopy (XPS) or Auger electron spectroscopy (AES).[7]

Passivated catalysts are often placed under reductive pretreatment conditions prior to reaction for the purpose of 'activation.' Leary and coworkers[35] reported the mobility of catalyst heteroatoms, primarily oxygen and carbon, during activation treatments. Reductive pretreatments could not solely remove oxygen deposited during passivation without concurrently removing lattice carbon as evinced by CO and CO_2 evolution during activation protocols; alterations in heteroatom removal caused by varying activation protocols distinctly affected the rates of deactivation of carbide catalysts for ethylene hydrogenation.[35] These studies demonstrate the difficulty in both synthesizing the desired catalytic molybdenum formulation and ascertaining the stoichiometry and uniformity of the catalyst surface in terms of Mo, O, or C terminations.

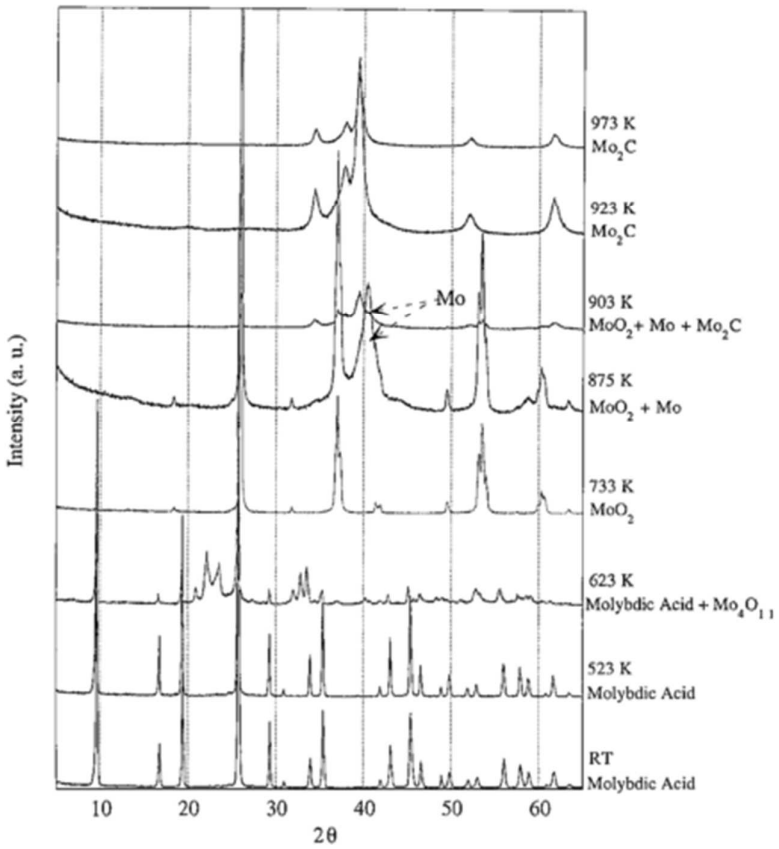

Figure 1. X-ray diffractograms showing the evolution of crystallographic structure of interstitial molybdenum compounds during the temperature programmed carburization of molybdic acid in 10 vol% CH_4/H_2, molar hourly space velocity of 68 h^{-1}. Samples were passivated at room temperature with pulses of O_2/He prior to XRD analysis. To obtain the two patterns of Mo_2C shown at the top of the figure, the carburization conditions were maintained for 1 h at the final temperature. Reprinted from Ref. 7, Copyright (2000), with permission from Elsevier.

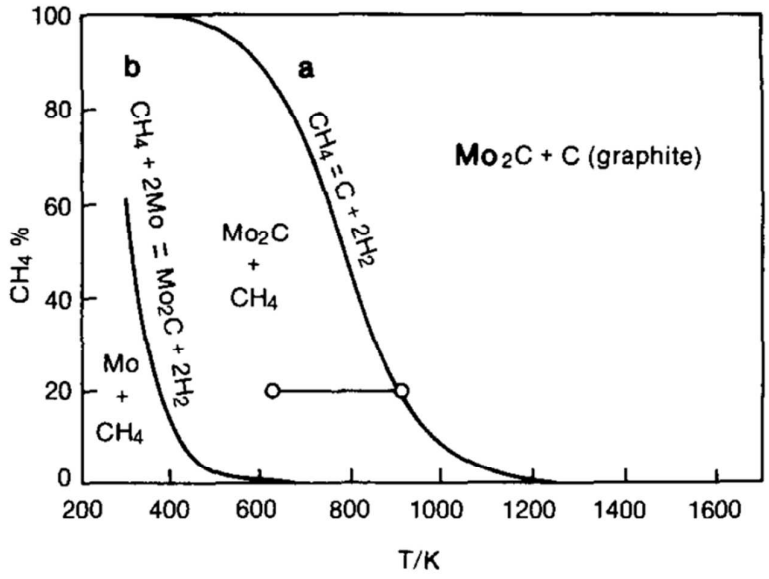

Figure 2. Equilibrium relationships at atmospheric pressure for the reactions (a) C(graphite) + 2 H_2 ↔ CH_4 and (b) Mo_2C + $2H_2$ ↔ 2Mo + CH_4. Reprinted from Ref. 49, Copyright (1987), with permission from Elsevier.

3.2. UHV Synthesis of phase-pure molybdenum carbides

Madix and coworkers developed a carbide synthesis method under UHV conditions via ethylene carburization of a clean Mo foil.[50] Chen and coworkers used this technique to carburize a crystalline Mo (110) surface until a surface C:Mo ratio of 0.4–0.6 was reached as assessed by AES.[18,51,52] This foil exhibited ethylene dissociation pathways characteristic of close-packed Pt-group metals, evincing the formation of a clean Mo_2C surface under UHV conditions with noble-metal-like characteristics noted to be distinct from pure Mo.[47] This synthesis technique can also be used for synthesizing phase-pure WC foils as demonstrated by Chen and coworkers,[53] and this method importantly allows for the characterization of the carbide surface using XPS, AES, high-resolution electron energy loss spectroscopy (HREELS), and UHV temperature programmed desorption (TPD). In situ UHV synthesis thus allows the complications of kinetic and thermodynamic limitations involved in a TPR synthesis to be circumvented, and the absence of an oxide precursor and constant flow of carburizing gas mixture allows for a phase-pure carbide product compared to a TPR

synthesized carbide which may have excess surface carbon or residual surface oxygen present.

4. Multifunctional catalytic activity and surface evolution

The varying synthesis protocols, from UHV to TPR synthesis, including the free variables during TPR synthesis of Mo-precursor, carburizing gas composition, temperature ramp rates and hold times, and passivation and activation procedures, all cause heterogeneity in the active catalyst surface and bulk stoichiometries. This heterogeneity results in binding sites whose structure and function vary and in turn allows for the broad spectrum of catalytic reactions discussed below to occur over these carbide surfaces.

4.1. Hydrogenolysis

Molybdenum carbide catalytic formulations have been reported to mimic noble-metal-like activity, especially the ability to activate hydrogen and hydrogenolyze C-C bonds.[1,2,9,54,55] Sinfelt and coworkers[47] reported temporal augmentation of ethane hydrogenolysis over a pure molybdenum sample at 668 K over the course of 6 h time-on-stream, discovering this activity evolution was due to the formation of a catalytic carbide phase as evinced by the appearance of Mo_2C peaks in X-ray diffractograms. Qi and coworkers[56] investigated ethane hydrogenolysis using DFT-modeled fcc and hcp Mo_2C crystal structures. The Mo-terminated surfaces of both crystals were active for hydrogenolysis of the C-C bond; hydrogen adsorbed on the catalyst surface was also able to reduce the activation barrier of the rate-determining C-C scission of the C_2H_5 intermediate. CH_3 and CH_2 species bound to both the fcc and hcp Mo_2C phases on top, hollow, and bridging sites with binding energies between -3.27 and -5.77 eV, demonstrating the extreme thermodynamic favorability of carbon to cover a Mo-terminated surface.

Frank and coworkers[57] investigated propane reactivity over an hcp Mo_2C surface using in situ XPS. Propane hydrogenolysis was prominent over the fresh carbide surface under reactant flow at 0.3 mbar, but surface coking deactivated these sites; this could be indicative of a stoichiometric and non-catalytic reaction. Similar results were observed by

Pham-Huu and Ledoux[9,55] when studying n-hexane hydrogenolysis over Mo_2C, by Neylon[53] when studying butane hydrogenolysis, and by Riberio[10] when studying n-hexane hydrogenolysis over WC_x catalysts. Ribeiro and coworkers[10] oxidized WC_x catalysts with dilute oxygen at room temperature for initial passivation; the passivated carbides were then exposed to 20 kPa O_2 and heated to 300-800 K and finally treated under H_2 at 673 K for 2 h before reaction. Oxidized WC_x formulations catalyzed n-hexane hydrogenolysis at 630 K with a constant turnover frequency as normalized by post-reaction ex situ CO chemisorption site densities even though oxygen modification of these samples decreased CO site density by a factor of ~4. These reports all noted that the highly reduced carbide catalyzed hydrogenolysis reactions and deactivated over time, and oxidative treatment of these catalysts suppressed hydrogenolysis activity.

These studies stress the importance of carbide surface termination and its effects on reactivity through synthesis, pretreatment, and transient reaction conditions. Specifically, the metallic hydrogenolysis activity appears most prevalent on clean, metal-terminated carbide surfaces and suffers from prominent deactivation, most likely due to coking and/or surface carburization as evinced by the extremely favorable carbon binding energies to metal-terminated carbides.

4.2. Hydrogenation

Mo_2C has been investigated for the catalytic hydrogenation of CO and CO_2 in studies using DFT calculations, surface science studies, and microreactor studies with pressures ranging from ambient to 7.0 MPa.[2–6,8,17,34,58–60] Wang et al.[33,34] used DFT to calculate favorable binding sites of CO and H_2 on Mo-terminated carbide surfaces; the strengths of H_2 and CO binding on hollow, bridging, and atop sites depended strongly upon the exposed crystal plane, temperature, pressure, and the gas phase composition. Wang and coworkers[34] used a microkinetic model involving the adsorption, desorption, and atomic CO dissociation over five different Mo_2C surfaces at 600 K and 40 bar CO pressure and reported that the activation of CO varied based on surface termination. CO adsorption was rate-determining on C-terminated surfaces, whereas adsorption was rapid and C-O dissociation was rate-limiting on Mo-terminated surfaces. Chen and coworkers[60] reported Mo_2C-catalyzed CO_2

hydrogenation to form CO and CH_4 at atmospheric pressure in a flow system, experimentally demonstrating CO_x hydrogenation on Mo_2C formulations.

Molybdenum carbides have also been reported to show metallic characteristics in hydrogenation of alkenes and aromatics with turnover frequencies comparable to those of noble metals.[46,61–64] Choi[64] reported that Mo_2C-catalyzed benzene hydrogenation was extremely dependent upon residual oxygen; oxidation decreased both the density and the strength of benzene hydrogenation active sites as measured by a CO chemisorption-normalized site-time-yield (STY) for benzene hydrogenation. A final synthesis temperature of 1023 K, compared to a typical synthesis temperature of 873 K, was necessary to fully remove all surface oxygen, and this 1023 K-synthesized catalyst also demonstrated the highest benzene hydrogenation site time yield (0.081 s^{-1} at RT). Frauwallner[62] and Ardakani[65] also reported Mo_2C-catalyzed toluene and tetralin hydrogenation where toluene hydrogenation was stable for over 1000 hours on stream.

Lee et al.[66] observed that the hydrogenation of benzene to cyclohexane over a freshly prepared Mo_2C catalyst was eliminated after ~3 h of anisole HDO reactivity, and this reduction in benzene hydrogenation was nearly irreversible. This change in reactivity was postulated to be the result of surface oxygen adatom (O*) deposition, mirroring the effects observed by Choi[64] of increasing benzene hydrogenation as a function of O* removal. These reports highlight the variability of the surface state of molybdenum formulations, most notably the effects of surface O*.

4.3. Isomerization

Catalytic alkane isomerization is a multifunctional process involving alkane dehydrogenation and acidic isomerization of the resulting alkene, subsequently followed by metallic hydrogenation to produce the isomerized alkane.[67] Ledoux and coworkers[45] designated the formation of a distinct oxycarbidic phase as being responsible for alkane isomerization activity. This necessary incorporation of oxygen to account for the presence of acidic activity falls in line with the work of Iglesia et al.[11] over bifunctional tungsten carbides, noting the presence of acidity that directly correlated with the oxidation of oxophilic tungsten catalysts. We also demonstrated the development of Brønsted acidity on Mo_2C catalysts with

the introduction of an O_2 co-feed by selective Brønsted acid titration during isopropanol dehydration using 2,6-di-tert-butylpyridine at varying acid site densities.[68] O_2 co-feed could reversibly tune dehydration rates by a factor of ~30 while the activation energy and turnover frequency for dehydration were invariant, leading us to attribute the tunable dehydration rate solely to Brønsted acid site density.

Neylon et al.[54] synthesized molybdenum carbide catalysts using a TPR method under H_2/CH_4 flow. These Mo_2C catalysts showed butane dehydrogenation and hydrogenolysis rates that were 144 and 78 times larger than concurrent isomerization rates, respectively. The carbides were treated under flowing H_2 at 753 K (activated) in order to remove surface oxygen before butane reactions; the dearth of surface oxygen due to the activation treatment could cause a lack of surface acidity that would lead to the observed low isomerization rates. The bifunctionality of oxophilic molybdenum carbide formulations is attributable to varied catalytic surface terminations including oxidation-induced acidity and carbidic metallic functionalities.

5. Hydrodeoxygenation

Investigation into hydrodeoxygenation has seen a recent surge due to motivations for using biomass as a renewable, sustainable carbon source for chemicals and fuels.[17,36,38,39,69–73] There are inherent challenges present in HDO; chemistries prevalent in hydrodeoxygenation of biomass-derived carbon sources necessitate the ability to selectively cleave C-O bonds from a diverse array of oxygen functionalities while preserving C-C bond integrity. HDO also requires H_2 activation while concurrently avoiding excessive hydrogenation of olefin and aromatic products and intermediates. Inherently multifunctional molybdenum carbide catalysts lend themselves to the complexities of HDO chemistries, and these functionalities are largely controlled by the surface composition, oxidation states, and available binding sites of these Mo_2C formulations as a function of the applied synthesis, pretreatment, and reaction conditions.

5.1. UHV deoxygenation

Chen and coworkers[18,19,52] used UHV-synthesized Mo_2C to investigate tunability of C-C and C-O bond scission using TPD, HREELS, and DFT calculations. UHV studies noted that biomass-derived probe molecules such as ethanol, furfural, and propanal could be deoxygenated over Mo_2C surfaces, although 17–62% of oxygenate conversion resulted in complete atomic decomposition to form surface adatoms or reforming pathways to produce CO, H_2, and surface C. Deoxygenation of these molecules was typically stoichiometric, possibly non-catalytic, as defined by a total reactivity of ~0.1 reactant molecules per surface metal atom.

The deoxygenation of propanol and propanal was proposed to traverse through a η^1(O) or η^2(C,O) mediated pathway; distinguishing between which surface conformation was prevalent was difficult due to the disappearance of HREELS bands at both 663 and 1711 cm^{-1}, associated with CCO deformation and C=O stretching, respectively, upon heating from 100 to 200 K.[18] McBreen and coworkers[74,75] used reflection-absorption infrared spectroscopy (RAIRS) to analyze UHV-synthesized Mo_2C dosed with oxygenated molecules and reported similar results. C=O scission of cyclopentanone and cyclobutanone was observed with subsequent formation of surface Mo-oxo and Mo-cycloalkylidene species. The cyclobutanone-dosed Mo_2C surface was heated until 1400 K, and cyclobutanone was observed to desorb from 900-1200 K; this high temperature desorption is indicative of a recombinative pathway distinct from simple molecular desorption typically observed below 400 K. The surface species formed upon dissociation of the ketone were identified via the characteristic Mo-oxo band at 950 cm^{-1} and the alkylidene band observed at 1130 cm^{-1}; bands at 1130 cm^{-1} are in close agreement with reported Ti-neopentylidene stretches.[75] Siaj et al.[74] observed the η^2(C,O) adsorbed state of cyclopentanone on the Mo_2C surface directly preceding C=O scission and alkylidene formation; both η^1 and η^2 binding modes were noted via RAIRS, and the elimination of all characteristic η^1 bands led to another intermediate state that preceded alkylidene formation. This alkylidene was then shown to undergo olefin metathesis with propylene, forming methylidene cyclopentane and ethylidene cyclopentane.

While these UHV techniques using a clean carbide surface give valuable insight into the reactivity of stoichiometrically pure carbidic formulations for oxygenate binding and deoxygenation pathways, it must be noted that the extreme oxophilicity and propensity for heteroatom adsorption and diffusion under synthesis and reaction conditions might lead to stoichiometric and non-catalytic reactivity under UHV reaction conditions due to surface and

sub-surface catalyst evolution as a function of time on stream. Insights gained from these stoichiometric reactions could aid in understanding observed catalytic induction periods of HDO reactions over Mo_2C catalysts under ambient or elevated pressures.

5.2. Hydrogenolysis-mediated HDO

We studied HDO of anisole[66] and furfural[76,77] over Mo_2C formulations that were initially passivated in 1% O_2 flow at ambient temperature and subsequently reactivated under 100 sccm H_2 for one hour at ~773 K. Vapor phase anisole HDO at 423 K and ambient pressure over self-supported Mo_2C was shown to be nearly 90% selective to benzene formation from 420-520 K with ~0.15 kPa anisole feed, demonstrating selective deoxygenation without aromatic hydrogenation. Lee et al.[66] reported that benzene synthesis rates had a zero order dependence on anisole pressure and a concurrent half order pressure dependence on hydrogen; anisole dependence remained zero order at all experimental conditions employed and H_2 pressure dependence remained ~0.5 order with anisole co-feed pressures varying from 0.1 – 1 kPa. A surface-mediated Langmuir-Hinshelwood-type rate expression involving any combination of two surface species could only show these dependencies if two distinct catalytic sites exist on the Mo_2C surface.

Benzene turnover frequency (TOF), as normalized by ex situ chemisorption measurements, ranged from 2.6 – 5.7 $mol_{benzene}\ mol_{CO\ site}^{-1}\ s^{-1}$ over a range of 51 – 208 μmol g^{-1} evincing that anisole HDO is metal-catalyzed and scales with the number of sites titrated by CO. Cyclohexane and other aromatic hydrogenation products of steady state anisole HDO accounted for <10% of the total carbon selectivity, and space velocity experiments demonstrated that these hydrogenation products were not primary products.

Phenol HDO via direct C-O hydrogenolysis was also studied by Boullosa-Eiras et al.[26] over Mo_2C catalysts at 623–673 K under 25 bar H_2, achieving ~90% selectivity to benzene and ~10% selectivity to hydrogenated aromatic products (cyclohexene + cyclohexane). We have recently reported that mixtures of aromatic oxygenates comprising anisole, m-cresol, guaiacol (GUA), and 1,2-dimethoxybenzene (DMB) can be selectively deoxygenated to form benzene and toluene with combined 90% yield over activated Mo_2C catalysts at ambient pressure and 553 K (Figure 3).[78] Toluene molar ratio, defined as moles of

toluene divided by moles of toluene and benzene, in HDO of these mixtures was found to increase proportionately from 4% to 66% as m-cresol molar composition varied from 0% to 70%.[78] These reports illustrate that molybdenum carbides can selectively and quantitatively cleave aryl-oxygen bonds and that transalkylation reactions are largely absent under the reaction conditions employed.

These direct C-O scission pathways are distinct from the noble metal-catalyzed phenol HDO pathway reported by Zhao et al.[37] which proceeds through aromatic hydrogenation followed by sequential dehydration and further alkene hydrogenation over Pd/C catalysts in presence of aqueous H_3PO_4. These reports note that Mo_2C-catalyzed HDO both preserves reactant aromaticity and conserves H_2, likely as a function of catalyst surface O* modification as described in Section 4.2 above, and selectively cleaves aromatic C-O bonds.

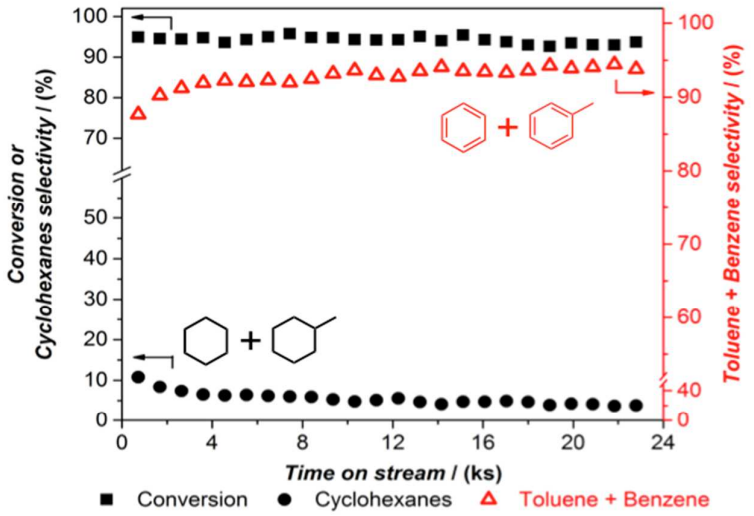

Figure 3. Conversion and product selectivity for HDO of a phenolic compound mixture over ~0.02 g Mo_2C. Molar ratio of m-cresol: anisole: DMB: GUA = 1: 0.96: 0.95: 0.98; Feed = phenolic mixture (0.03)/ H_2 (91)/ He balance (mol%) at 114 kPa total pressure and at 553 K; space velocity 198 $cm^3\ s^{-1}\ g_{cat}^{-1}$; ex situ CO uptake = 124 μmol g_{cat}^{-1}; Cyclohexanes contains methylcyclohexane and cyclohexane. Reproduced with permission from Ref. 78.

5.3. Metallic-acidic bifunctional HDO

Complex aromatic oxygenates such as phenol, anisole, m-cresol, and guaiacol are often studied as probe molecules for lignin-derived bio oil valorization.[24,37,79–84] Mortensen et al.[84] reported reactions of phenol/octanol mixtures in a continuous flow system over Mo_2C/ZrO_2 under 100 bar H_2 pressure and at temperatures of 553–653 K. Higher conversion, obtained by increasing temperature, favored the formation of benzene, whereas lower conversion favored formation of acid-catalyzed products such as octene and octyl phenyl ether. Octyl phenol, most likely the result of Brønsted acid catalyzed transalkylation, was the dominant product with ~70% yield at full phenol conversion. The ZrO_2 support was tested to show acidic activity as evinced by catalyzing octene, octyl ether, octyl phenol, and octyl phenyl ether formation in absence of Mo_2C; whether observed acidic catalysis over Mo_2C/ZrO_2 was partially due to O*-Mo_2C moieties or entirely due to the acidic ZrO_2 support is unclear from this report.

The octyl phenol product in the work of Mortensen[84] is depicted as ortho-substituted 2-octyl phenol; this supplements the findings of Jongerius et al.[24] who noted the formation of ortho- and para-cresol upon guaiacol HDO under 55 bar H_2 pressure in a batch system at 573-648 K over Mo_2C/carbon nanofiber (CNF) catalysts as shown in Scheme 2(a). The aryl–OH substitution of phenol is postulated to act as an o,p-directing agent in the electrophilic addition of residual surface methyl groups residing over O*-Mo_2C Brønsted acid sites as a result of guaiacol HDO to form phenol, producing ortho- and para-cresol. These results from Mortensen[84] and Jongerius[24] suggest that Brønsted acid sites exist on Mo_2C catalysts even under hydrotreatment conditions of 55–100 bar H_2 and 573-653 K as well as the ability of these acid sites to catalyze transalkylation and maintain desirable carbon chain growth.

Complex triglyceride-derived C_{18}^+ probe oxygenates such as alkyl stearates and stearic, oleic, and linoleic acids that necessitate bifunctional HDO have also been studied for HDO over molybdenum carbide catalytic formulations.[85–89] Stellwagen and coworkers[85] studied reactions of stearic acid over CNF-supported Mo_2C and W_2C in a batch reactor system at 30 bar and 573–623 K. As a function of reaction time, octadecanal and octadecanol were the first products to form from stearic acid reactions, followed by some intermediate formation of octadecene with 80% octadecane yield at the conclusion of the 3 h reaction. Primary conversion of the carboxylic acid to the aldehyde appears to be a metal-mediated C-O hydrogenolysis reaction, followed by metal-catalyzed aldehyde hydrogenation to form the alcohol. This alcohol can be subsequently dehydrated over acidic sites to form an alkene,

which undergoes sequential hydrogenation to form the alkane; this proposed reaction pathway is shown in Scheme 2(b). Acidic dehydration was attributed to MoO_x species observed in catalyst XPS measurements where >75% of surface Mo resided as Mo^{6+}. Catalysts were recycled and used in repeat stearic acid HDO experiments. A 30% decrease in stearic acid conversion was concurrent with the emergence of MoO_x peaks in post-reaction X-ray diffractograms. The presence of Brønsted acidity and the inhibition of aromatic hydrogenation, characteristics that are both suited for biomass HDO catalysis, have been attributed to mild Mo_2C surface oxidation, but Stellwagen and coworkers[85] also demonstrate the detrimental effects of excessive Mo_2C oxidation on stearic acid HDO.

Biomass probe molecules, ranging from lignin-derived aromatics to triglyceride-derived alkyl stearates, all either necessitate the metal-acid bifunctionality provided by oxygen-modified Mo_2C to promote complex oxygenate HDO or can benefit from both O*-suppressed aromatic hydrogenation and carbon chain growth pathways mediated via acid-catalyzed transalkylation reactions. This metallic/acidic interplay elicits comparison to interstitial carbide-catalyzed bifunctional isomerization observed by Ledoux, Iglesia, and Boudart,[10,11,45,67] evincing the presence of both metallic carbidic active sites and O*-induced surface Brønsted acidity. Unlike the strictly metal-catalyzed anisole HDO observed by Lee[66,77] and Boullosa-Eiras,[26] the acidic/metallic bifunctional balance that results from complex surface terminations is critical for complex oxygenate HDO.

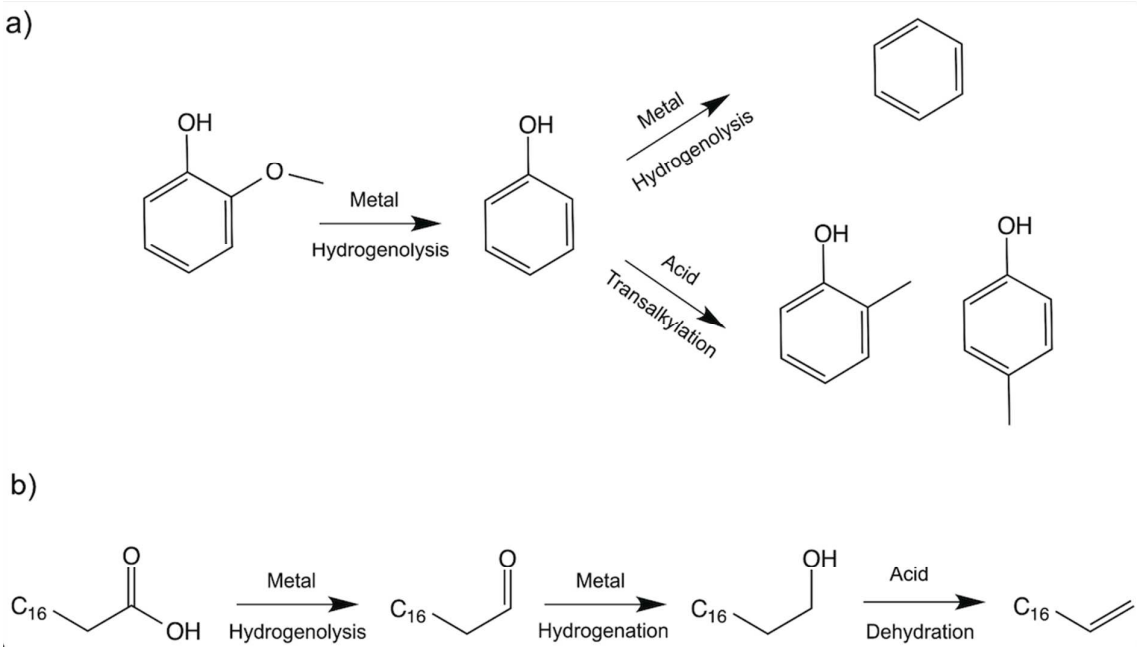

Scheme 2. (a) Hypothesized bifunctional HDO of guaiacol, demonstrating metal-catalyzed selective aryl C-O bond cleavage and Brønsted acid-catalyzed aromatic alkylation. Adapted from Ref. 24, Copyright (2013), with permission from John Wiley and Sons. (b) Sequential bifunctional HDO of stearic acid via metal-catalyzed hydrogenolysis and hydrogenation followed by acid catalyzed dehydration. Adapted from Ref. 85 with permission from the Royal Society of Chemistry.

5.4. Acidic deoxygenation via dehydration

We have reported the use of oxygen-modified molybdenum carbide catalysts for the deoxygenation of isopropanol to form propylene.[68] TPR synthesized Mo_2C catalysts at 873 K that were shown to have minimal bulk oxygen, as evinced by extended reduction under H_2 flow up to 1053 K that yielded negligible quantities of H_2O, were exposed to IPA/He flow. Initially, catalytic activity of these carbidic formulations was primarily metallic and alkaline; products formed involved dehydrogenation to acetone, acetone condensation to form diacetone alcohol, and further reactions of diacetone alcohol to form varied C_6^+ products. Propylene was formed with <5% carbon selectivity. Upon exposure to an O_2 co-feed, product carbon selectivity shifted to nearly 90% dehydration products (propylene and diisopropyl ether (DIPE)). The proposed metallic and acidic IPA conversion pathways are represented in

Scheme 3. Selective titration of propylene formation rates with a 2,6-di-tert-butylpyridine co-feed demonstrated that the observed deoxygenation of isopropanol to form primarily propylene via dehydration was the result of oxygen-induced Brønsted acidity on the carbide surface, yet surface oxidation did not alter the bulk structure of 2-5 nm Mo_2C crystallites as inferred from pre- and post-reaction XRD.

Matsuda and coworkers[90,91] observed similar dehydration product selectivities to propylene and DIPE over H_2-reduced MoO_3 and Pt/MoO_3. MoO_3 species reduced under flowing H_2 for 12 h at 623 K exhibited no induction period in propylene and DIPE formation rates; rates of formation of these dehydration products deactivated over time. The nature of the catalyst as a reduced molybdenum oxide, inferred from prominent MoO_2 X-ray diffraction peaks and monotonically decreasing Mo valence with increasing reduction temperature as measured by the consumption of O_2 necessary for re-oxidation to MoO_3, coupled with the lack of an induction period implicate the unlikelihood of in situ surface carburization affecting the observed acidic dehydration activity, further strengthening the claim of molybdenum oxide Brønsted acidic domains on the catalyst surface.

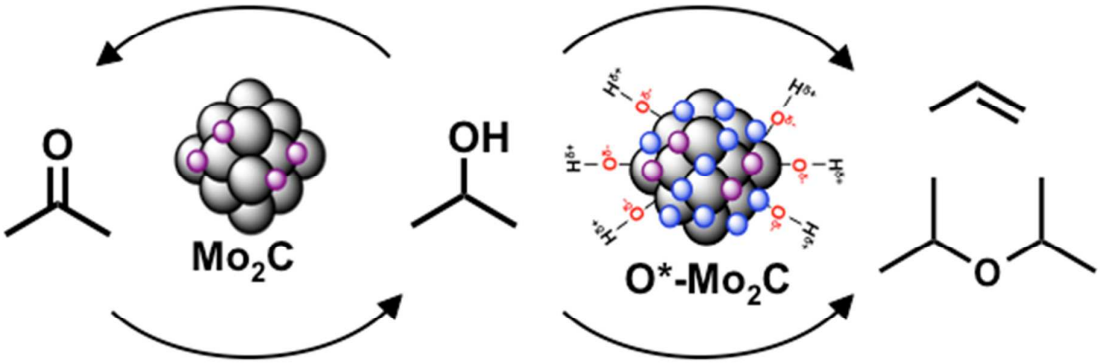

Scheme 3. Proposed reaction network for IPA over acidic and metallic Mo_2C sites.

5.5. The effects of water on molybdenum carbide catalysis

Water is ubiquitous in upgrading biomass to fuels and chemicals as bio-oil contains ~30 wt% of H_2O, and oxygen contained in biomass derivatives formed upon depolymerization/deconstruction of lignocellulosics is removed as water in HDO

chemistries.[69] The stability and activity of molybdenum carbides during deoxygenation reactions in presence of water, therefore, are important.

DFT studies have shown that H_2O can dissociate to OH* and H* (* represents an adsorption site), which can further dissociate to form O* and 2H* on β-Mo_2C(001),[92–94] consistent with the experimentally measured near zero order dependences on H_2O pressures for water-gas shift (WGS) over bulk Mo_2C.[95] Namiki et al.[96] demonstrated the dissociation of H_2O on carburized 4.8 and 8.5 wt% Mo/Al_2O_3 catalysts during WGS reaction, in which H_2, $^{13}C^{18}O$, $^{13}C^{18}O_2$ and $^{13}C^{18}O^{16}O$ were observed via mass spectrometry upon pulsing $H_2{}^{18}O$ into a continuous stream of ^{13}CO in He at 423 K. Ren et al.[19] showed using DFT calculations that adsorbed oxygen from oxygenates (O*) can be removed from a Mo_2C(0001) surface in presence of excess H_2 as hydrogen can dissociate onto an O*-occupied Mo_2C site to form OH*, which can subsequently react with another OH* to remove the adsorbed oxygen by forming H_2O* and O*, however, the activation barrier for OH* coupling is ~110 kJ mol^{-1}. Thermodynamic calculations show that $Mo_2C_{(s)}$ can be oxidized by both $H_2O_{(g)}$ and $H_2O_{(l)}$ to form MoO_2 ($\Delta G_{rxn,\ 573\ K}$ ~-20 and ~-130 kJ mol^{-1}, respectively), however, the oxidizing strength of O_2 ($\Delta G_{rxn,\ 573\ K}$ ~-1300 kJ mol^{-1}) is much stronger than that of H_2O.[69,84]

We recently reported that adsorbed oxygen on Mo_2C formulations, from oxygen-containing compounds including water, methanol, lignin-derived phenolics, or O_2, diminishes metallic functions[78] and generates acidic sites.[68] Hydrogenation rates of benzene and toluene on a passivated Mo_2C formulation that was H_2-treated at 573 K for 1 h prior to the reaction were completely inhibited in presence of a water co-feed, showing that the introduction of water to molybdenum carbide formulations can irreversibly inhibit the metallic hydrogenation function.[78] In situ synthesized Mo_2C was treated in 10 kPa of H_2O for 2.5 h before exposing the sample to isopropanol (IPA)/CH_4/He mixtures (1/3.5/Bal %) at 415 K and ambient pressure; dehydration rates to form propylene increased fourfold while the formation rates of C_6^+, which are metal/base catalyzed products, decreased by half compared to a fresh Mo_2C that had not been exposed to H_2O or O_2.[68] The effect of water treatment, however, is less severe than that noted upon exposing a fresh Mo_2C sample to O_2 (~13 kPa), which is accompanied by a temperature exotherm of ~100 K and concurrent elimination of C_6^+ formation rates in less than 20 min.[68] An independent experiment of 0.5 kPa IPA dehydration with 0.7 kPa of H_2O and 13.5 kPa of O_2 co-feed on a fresh Mo_2C demonstrated that water co-feed has no kinetic effects on IPA dehydration,[68] which is consistent with the

reported involvement of Brønsted acid sites generated on Mo_2C upon O_2 exposure.[68] The effect of water co-feed is minimal as oxygen co-feed (~13.5 kPa) is the dominating contributor to the formation of Brønsted acid sites for IPA dehydration. The negligible effect of H_2O on IPA dehydration is also consistent with the experimentally measured zero order dependencies on IPA;[68] the IPA-saturated Mo_2C surface (0.5 kPa) shows negligible IPA dehydration inhibition from a comparable water co-feed pressure (0.7 kPa), implicating that O*-induced Brønsted acid sites favor IPA adsorption over H_2O. No deactivation of Mo_2C was observed for at least 48 h on-stream when 31.8 mol % of water was co-fed with 5.7% CO during WGS reaction at atmospheric pressure between 493 K to 568 K and Mo_2C phases remained in the bulk structure as no oxide phases were observed from XRD patterns of the spent catalysts.[97,98] The time-on-stream stability for WGS reaction reported by Moon and coworkers[97,98] is presumably due to the surface dominating O*/*OH species derived from H_2O dissociation[92–95] participating in the catalytic cycle as has also been suggested by DFT calculations on β-Mo_2C(001).[94]

The inhibitive effect of water on aromatic hydrogenation is analogous to the oxidation-induced suppression of hydrocarbon hydrogenolysis discussed in Section 4.1 and contrasts the case studies on IPA dehydration and WGS reactions in which oxygenates are involved as reactants/products. We postulate that a more carbidic and less oxidized surface is required for catalytic hydrogenation and that reactant feeds devoid of oxygenates are necessary to retain this carbidic surface; adsorbed oxygen alters the surface stoichiometry and eletronic structure, thereby altering the adsorption properties of hydrocarbon reactants such as benzene and toluene. This oxidation-induced inhibition of hydrocarbon hydrogenation was also noted by Choi et al.[7] when studying the effect of carburization on benzene hydrogenation. The inhibitory effect of adsorbed oxygen on aromatic hydrogenation in conjunction with the selective Ar-O cleavage on O*-modified Mo_2C formulations results in the high selectivity of aromatics (>90%) in hydrodeoxygenation of lignin-derived phenolic compounds.[78]

Hydrothermal stability and activity of Mo_2C formulations for aqueous-phase hydroprocessing of acetic acid were studied extensively by Choi et al.[99] The bulk structure of molybdenum carbide formulations remained as hcp Mo_2C after hydrothermal treatment in liquid water under N_2 at 523 K and ~47 bar for 48 h, demonstrating that molybdenum carbide structures are resistant to bulk oxidation at high pressure liquid water conditions. Surface oxidation of the samples, however, was confirmed by XPS studies as the percentage of Mo

3d in Mo-O form increased fourfold after the hydrothermal treatment. Similar surface oxidation results were observed for a fresh Mo_2C tested for hydroprocessing (10% guaiacol in H_2O at 523 K and ~137 bar), suggesting that the oxidative effects of the guaiacol solution on the Mo_2C surface are comparable to that of pure water. Hydrothermal aging has a minimal inhibitory effect for acetic acid conversion (10 w/w % in H_2O at 523 K and ~137 bar) to ethanol and ethyl acetate under hydroprocessing conditions; acetic acid conversion remained constant at ~40% when using both a fresh carbide catalyst and a hydrothermally treated carbide catalyst. The authors also noted that structure and activity changes to molybdenum carbides due to hydrothermal conditions are sensitive to the original Mo_2C structure which mirrors the observed severe deactivation in HDO of phenol and 1-octanol on Mo_2C/ZrO_2 when 30% H_2O was co-fed.[84] The results for IPA dehydration, WGS reaction, and hydrodeoxygenation of acetic acid and guaiacol suggest that the surface modification of Mo_2C by O* is agnostic to the source of oxygen, namely phenolic compounds, fatty acids, alcohols, or water; these oxygenates can dissociate and leave behind O* on the surface, inhibiting the metallic function and potentially generating Brønsted acid sties. The major difference between the oxygen sources is that the oxidizing strength of O_2 is stronger than that of other oxygenates as demonstrated by the thermodynamic favorability of $Mo_2C_{(s)}$ oxidation using O_2 in reference to H_2O discussed above.

6. Tungsten-based catalytic formulations

Tungsten carbides and oxides have been investigated as catalysts for hydrogenolysis,[10,11] isomerization[11,67,100,101] and for deoxygenation reactions via HDO[22,23,53,85,102] and dehydration.[103] Maire and coworkers[100,104,105] and Iglesia and coworkers[10–12] investigated the effects of oxygen modification of WC_x catalysts. O_2-treated catalysts exhibited decreased metal-catalyzed hydrogenolysis areal rates and increased bifunctional metal-acid catalyzed alkane isomerization rates as described in Section 4.1. The O_2-induced Brønsted acidity necessary for alkane isomerization was hypothesized to be due to WO_x moieties generated on the oxophilic WC_x surface; even after oxidation, WC_x catalysts retained metallic activity capable of hydrogenolysis and hydrogenation.

Chen and coworkers used DFT, UHV TPD, and microreactor experiments to study HDO over WC catalysts.[53] WC synthesized at 1273 K catalyzed propanal and propanol HDO

at 653 K; HDO selectivities, most notably the dominant product of propylene, were consistent at ~60% over both WC and Mo_2C catalysts, yet HDO conversion was ~10-fold higher over Mo_2C as opposed to WC. This was hypothesized to be a function of catalyst particle size; WC final synthesis temperature in this work was 1273 K, and high temperatures result in more particle sintering and lower surface area compared to the 60-100 m^2 g^{-1} observed for Mo_2C catalysts synthesized with final synthesis temperatures of ~873 K.[49]

Bitter and coworkers investigated HDO of stearic acid over CNF-supported Mo_2C and W_2C.[85] Both carbides catalyzed HDO via metal-acid bifunctional pathways as mentioned in Section 5.3. W_2C/CNF catalyzed octadecanol dehydration under N_2 atmosphere to ~80% octadecene yields, and dehydration yields were almost identical to that catalyzed by WO_3/CNF due to acidic WO_x moieties in absence of carbidic WC_x sites. The oxophilicity of WC_x catalysts leads to the generation of acid sites similar in nature to those observed over oxygen-modified molybdenum carbides, but WC_x oxidation appears to be more extensive as evinced by greater dehydration and lower hydrogenation rates to form octadecane from octadecene over W_2C/CNF in comparison with Mo_2C/CNF catalysts. The generation of acidic character and diminution of metallic catalysis with increasing catalyst oxidation remains constant across the interstitial carbides catalysts WC_x and MoC_x; the evolution of catalytic functionalities of interstitial carbide catalysts are primarily similar although their varying oxophilicities affect the extent of oxidation and commensurately result in changes in the number and density of active sites on these materials.

7. Perspective

The diversity of catalytic functions exhibited by molybdenum and tungsten carbide arises because of both the structure and composition of the material and its evolution under reactive environments. Density functional theory calculations reveal that the binding energy of H_2 and CO on hexagonal Mo_2C is lower on the (101) surface relative to the (100), (201), and (001) surfaces with adsorption energies varying both with coverage and whether on-top, bridging, or hollow sites are involved in binding.[31,33] Along the same lines, oxygen binding energy on an Mo-terminated β-Mo_2C(001) surface is calculated to be ~3 eV stronger than that on a C-terminated (001) surface.[92] Experimental assessment of these surface characteristics is complicated by protocols for synthesizing and passivating these oxophilic

materials which can result in carbon deposition during hydrocarbon treatment, bulk carbon removal during reduction processes, and formation of sub-surface/surface-adsorbed oxygen during passivation or reaction.[7,8,35,43]

Both carburization and residual oxygen content describe the metal-like behavior of transition metal carbides.[7,49,106] The existence of surface carbon, a diversity of oxygen-binding sites, and carbon-deficient centers is evident from the detailed chemical characterization and kinetic studies of Ribeiro, Iglesia, and Boudart on fresh/oxygen-exposed tungsten carbide materials.[10–12] Hydrogenolysis rates, in particular, were noted to be 100-fold lower for samples that had been oxygen-treated.[12] Acid-catalyzed reaction pathways were concurrently promoted on oxygen-modified surfaces.[10–12] A similar tradeoff in catalytic functions between n-hexane hydrogenolysis and isomerization was reported by Guille and co-workers[9] on Mo_2C catalysts pretreated in oxidative environments. The evolution of structure and site density of Mo_2C formulations as a result of varying synthesis protocols is evident from the amount of residual oxygen content; the amount of water evolved during temperature-programed reduction experiments on as-synthesized molybdenum carbides decreased to negligible values when the carburization temperature for these materials increased from 923 K to 1023 K.[7] The resulting density of sites titrated by CO chemisorption and the benzene hydrogenation rate at room temperature normalized per CO chemisorption site increased from 2.5×10^{14} to 5.4×10^{14} cm^{-2} and from ~0.01 to ~0.08 s^{-1}, respectively.[7]

The evolution of surface composition and structure occurs not only with synthesis protocols but also with the reaction environment. Oxygen composition in molybdenum carbides was noted to vary with hydrocarbon treatments; Reimer and coworkers[8] used elemental analysis to reveal that negligible quantities of oxygen remained in a bulk molybdenum carbide after catalytic C_2H_6 hydrogenolysis whereas O/Mo = 0.44 was measured in a catalyst that underwent pretreatment in CH_4/H_2 mixtures. Emerging research on the synthesis of carbon nanotubes on cobalt surfaces has established that surface depletion of carbon occurs in these materials, implying that bulk and surface structure heterogeneity in composition may exist during reaction conditions.[107,108] Similar characteristics were observed in MoO_3-derived formulations as reported by Matsuda and coworkers.[90] Partial reduction of Pt/MoO_3 catalysts led to both an increase in surface area from ~5 to ~250 m^2 g^{-1} and a change in the average Mo valence from ~4 to ~2.[90] The catalytic function of Pt/MoO_3 formulations for heptane isomerization evolved correspondingly and a maximum in isomerization activity

at a reduction temperature of 723 K was noted. Both isomerization and dehydration activities being nearly invariant among H_2-reduced Pt/MoO_3 and $H_{1.55}MoO_3$ and isomerization selectivity being the same for different Mo valence states that varied from 0.4 to 2.8 on Pt/MoO_3 formulations suggest that similar catalytic centers exist on oxidic molybdenum surfaces across a range of bulk compositions.[90] Along the same lines, Román-Leshkov and coworkers[25] have recently shown that structural characteristics of MoO_3 catalysts evolve during HDO catalysis of phenolic compounds which results in the formation of oxycarbide or oxycarbohydride ($MoO_xC_yH_z$) phases.

Hydrodeoxygenation chemistries on carbidic catalysts and specifically on Mo_2C-derived materials exhibit each of the characteristics noted above. Surface science studies using C_2-C_3 oxygenates containing C-OH and C=O groups show that oxophilic Mo_2C or tungsten carbidic formulations selectively cleave the carbon-oxygen bond,[18,19,52,53] and oxygen accumulation on the Mo_2C surface was observed via Auger electron spectroscopy after deoxygenation of propanal, 1-propanol, furfural, or furfural alcohol.[18] Computational chemistry studies report that oxygen binding energies on both Mo- and C-terminated orthorhombic $Mo_2C(001)$ exceed 5 eV,[92] at least three times larger than that for molecules like CO, CO_2, H_2, or H_2O, and the removal of adsorbed oxygen is unfavorable with activation barriers exceeding 2 eV.[19] These reports suggest that it is unlikely for a purely carbidic surface to exist under hydrodeoxygenation reaction conditions.

Chemical transient studies on as-synthesized Mo_2C formulations for anisole HDO at atmospheric pressure reveal that cyclohexane is formed in an initial transient, however, concurrent oxygen accumulation of ~0.3 monolayer (ML) results in almost complete inhibition of cyclohexane formation in benzene hydrogenation reactions.[109] These chemical transient studies also showed carbon deposition equivalent to ~0.9 ML of C_6 on the surface upon initial exposure to anisole/H_2 mixtures, suggesting the existence of carbon-deficient centers and surface carbon species on the catalyst.[109] A separate experiment demonstrated that benzene hydrogenation on as-prepared Mo_2C formulations was significantly suppressed when the reactant feed was switched from benzene/H_2 to anisole/H_2 mixtures. Cyclohexane formation rate did not recover even after the reactant feed was switched back to benzene/H_2.[66] We postulated that oxygen atoms were irreversibly deposited on the surface from anisole HDO and inhibited benzene hydrogenation; this is consistent with our report where we noted that the introduction of water or methanol resulted in the nearly complete

inhibition (>95%) of benzene and toluene hydrogenation on Mo_2C formulations.[78] These surface science, computational chemistry, and chemical transient studies allow us to infer that the catalyst composition for atmospheric HDO is likely an oxygen-modified carbide, most likely an oxycarbide, although the structure and composition of the active catalytic species under reaction conditions cannot be ascertained.

The dynamics of catalyst composition and function under reactive environments necessitates the use of in situ probes of structure and site density while it limits the use of elemental analysis, probe molecule spectroscopy, and structural characterization methods that transiently expose the catalyst to oxygen-containing or reducing environments. We report the use of competitive CO adsorption during anisole hydrodeoxygenation reactions, in which CO acts as a reversible titrant, to accurately assess the number of catalytic sites in situ (Figure 4 (a)).[109] The assessment of the number of catalytic sites involves a transient experiment which can be rigorously interpreted with the assumptions that one CO adsorbs per active site[7] and that all active sites have similar activity after eliminating any contribution from parallel water-gas shift and/or CO methanation reactions. A total of 31 such CO titrations at varying CO space times (Figure 4 (b)), defined as the amount of catalyst divided by the CO co-feed flow rate, allowed us to infer that only ~10% of the sites measured by ex situ CO chemisorption are active for catalysis under anisole HDO conditions, as benzene turnover rates (TOR) normalized by the number of in situ CO sites are an order of magnitude larger than those normalized by the number of ex situ CO sites, $\sim 2\times10^{-3}$ mol s^{-1} $mol_{\text{in situ CO site}}^{-1}$ and $\sim 2\times10^{-4}$ mol s^{-1} $mol_{\text{ex situ CO site}}^{-1}$, respectively.[66,109] The difference in the number of sites could either be a consequence of changing surface area and accessibility of the active centers in presence of oxygen-containing species or an ensemble effect for anisole HDO.

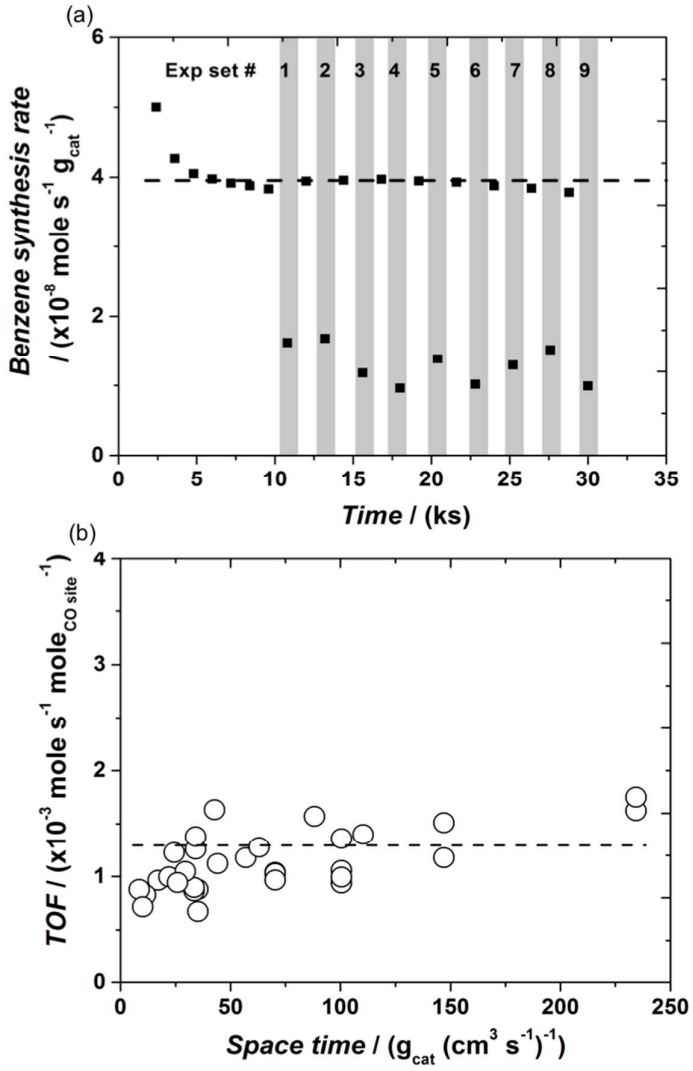

Figure 4. (a) Benzene synthesis rates versus time-on-stream during the course of in situ CO titration. The catalyst (~1.11 g_{cat}, CO chemisorption uptake ~240 μmol g_{cat}^{-1}) was stabilized for ~10 ks before in situ CO titration. Shaded areas indicate CO/Ar mixtures (~0.005–0.028 $cm^3\ s^{-1}$/ ~0.036 $cm^3\ s^{-1}$) were co-fed into the reactant feed comprising anisole/ H_2 (vol %) = ~0.36/bal with a total flow rate of ~1.67 $cm^3\ s^{-1}$ at reaction temperature ~423 K and under ambient pressure. (b) Turnover frequency (TOF) of benzene synthesis determined by in situ CO titration as a function of CO space time, defined as (amount of catalyst)/(CO cofeed flow rate employed in the corresponding titration experiments). Different CO space times were achieved using both different amounts of catalyst (~1.77, ~1.11, ~0.43 g) and different CO cofeed flow rates (~0.0076−0.053 $cm^3\ s^{-1}$).[a] The dashed lines are shown as a guide to the eye. Reprinted with permission from Ref. 109. Copyright (2015) American Chemical Society.

The effects of chemisorbed oxygen on catalytic and chemisorptive properties of tungsten carbide materials were examined by exposing fresh carbide samples to O_2 at varying temperatures followed by H_2 treatment at 673 K.[10–12] Iglesia and coworkers[10,11] reported a systematic inhibition of hydrogenolysis rates and a concurrent increase in the rate of acid-catalyzed reactions for such oxygen-modified formulations, demonstrating the bifunctionality of transition metal carbides. We report that selectivity in HDO is systematically and significantly altered by chemisorbed oxygen. Oxygen-exposed Mo_2C samples were prepared in a manner similar to that reported by Ribeiro, Iglesia, and Boudart and coworkers.[10–12] The selectivity of these formulations for HDO of anisole is shown in Figure 5 where the O/Mo_{bulk} content was assessed by temperature programmed reduction in H_2/Ar flow to 723 K. As-synthesized Mo_2C formulations prepared by treatment in CH_4/H_2 mixtures, without exposure to air, resulted in ~1% phenol selectivity and ~90% benzene selectivity. Oxygen-treatment of these samples systematically altered benzene and phenol selectivity to be less than 20% and greater than 80%, respectively, which is a consequence of the concurrent decrease in benzene synthesis rates from 6.8×10^{-8} to 0.1×10^{-8} mol s^{-1} g_{cat}^{-1} and an increase in phenol synthesis rates from 0.1×10^{-9} to 7.8×10^{-9} mol s^{-1} g_{cat}^{-1}. The synthesis rates and product selectivity are stable for ~4 days on-stream after an induction period of ~8 h under the reaction conditions investigated. Benzene TORs measured by in situ CO titration on the four samples were found to be invariant with the amount of oxygen incorporated, demonstrating that oxygen chemisorption on Mo_2C formulations alters the number, not the identity, of the active sites for benzene synthesis. Phenol sites on all samples, however, were not titrated by CO co-feeds; therefore, we cannot conclude whether the low phenol synthesis rates are stoichiometric or catalytic. These changes in rates and selectivity may arise due to both composition/structure changes as well as changes in the electronic and chemisorptive/reactive properties of these formulations.

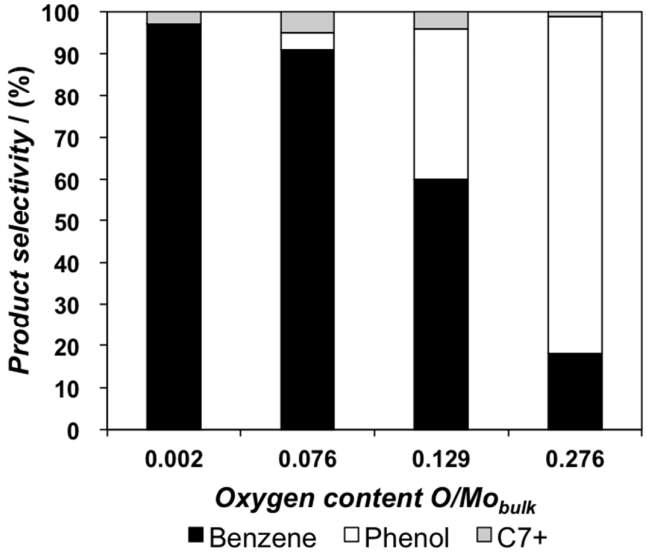

Figure 5. Product selectivity for anisole hydrodeoxygenation on the as-synthesized fresh and oxygen modified Mo_2C formulations at 423 K and ambient pressure. Feed is comprised of anisole/ H_2 (mol %) = ~0.56/bal; space velocity ~1.68 cm^3 s^{-1} g_{cat}^{-1} and 0.99 g_{cat} catalyst.

Oxygen-modification of tungsten and molybdenum carbidic formulations, of particular relevance to deoxygenation chemistries, leads to a mitigation of metallic characteristics while concurrently engendering acid character to the catalyst (Scheme 4). We note that hydrogenation rates over metallic sites on Mo_2C formulations decrease with O_2 treatment; molybdenum carbide catalysts that were exposed to 13.5 kPa O_2 for ~4 h were nearly inactive for acetone hydrogenation. The balance between metallic and acidic functions can be adjusted to primarily acidic upon co-feeding oxygen. Co-feeding 0–13.5 kPa O_2 flow to an isopropanol stream over a fresh Mo_2C catalyst resulted in a ~30 fold increase in the rate of isopropanol conversion to propylene per gram of Mo_2C.[68] This increase in rate was not accompanied by a change in the measured reaction order and activation energy or in bulk structural changes of the Mo_2C as evinced by X-ray diffraction. In situ chemical titration using 2,6 di-tert-butylpyridine revealed that Brønsted acid site densities increase with increasing O_2 pressure, and isopropanol dehydration rates are invariant when normalized rigorously to the acid site density (Figure 6).[68] We posit that O_2 co-feed on Mo_2C results in the formation of Brønsted acid sites similar to those theorized by Chia et al.[110] for Re/Rh formulations that arise due to the oxophilic nature of Re.

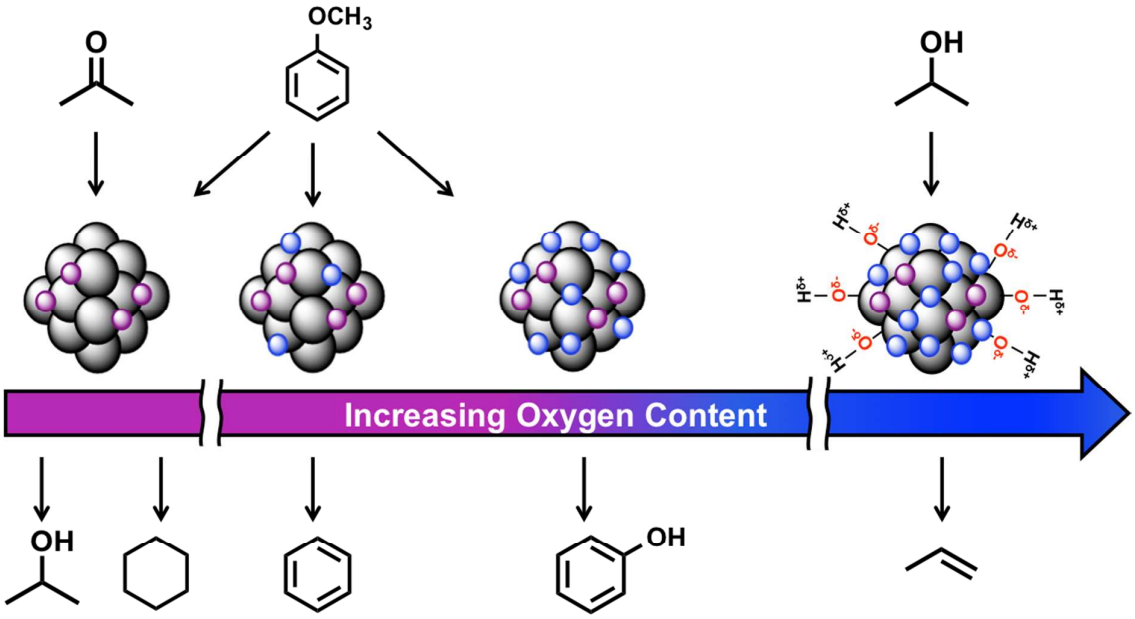

Scheme 4. The evolution of molybdenum carbide functionality with increasing oxygen content.

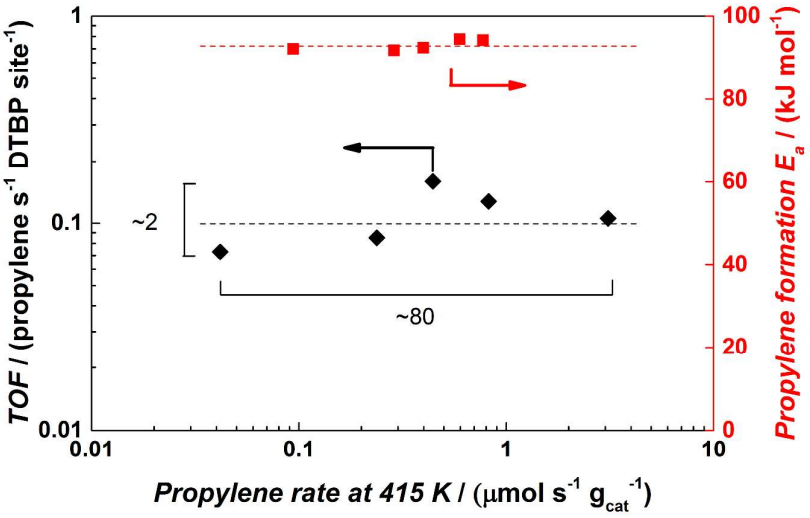

Figure 6. Propylene turnover frequency (TOF) (◆) and activation energy of propylene formation (■) as a function of propylene synthesis rate normalized by catalyst loading. Propylene rates per gram were manipulated with O_2 co-feed variation from P_{O2} = 0–13.5 kPa, and TOF was calculated using Brønsted acid site density measured by in situ DTBP titrations. Reaction conditions for propylene synthesis rate at 415 K: ~0.29 g_{cat}, P_{Total} = 114 kPa, P_{IPA} =

1–2 kPa, P_{CH4} = 4 kPa (internal standard), balance He, space velocity of 6.9 cm^3 s^{-1} g_{cat}^{-1}. Reaction conditions for measuring activation energy: T = 405–438 K, ~0.015 g_{cat}, P_{Total} = 114 kPa, P_{CH4} = 4 kPa (internal standard), balance He. Space velocity of 133 cm^3 s^{-1} g_{cat}^{-1}. Adapted with permission from Ref. 68.

In summary, emerging research has clearly demonstrated the potential of transition metal carbidic formulations as hydrodeoxygenation catalysts at low pressure and temperature. Two characteristics of metal carbide formulations, namely the high selectivity for C-O bond cleavage and the near absence of sequential hydrogenation reactions on oxygen-modified materials, distinguish them from noble metal or hydrotreating catalysts. The oxophilic character of these carbidic materials engenders both bifunctionality and selectivity for hydrodeoxygenation catalysis and is likely the primary characteristic to correlate change in catalyst function under reactive environments. The evolution of morphology, surface composition, and catalytic function under oxidative environments renders unique challenges for structural and chemical characterization of these materials and highlights the critical importance of in situ chemical transient and chemical titration studies for assessing the site requirements in these materials.

Acknowledgements

We acknowledge financial support from Office of Basic Energy Sciences and the U.S. Department of Energy under award number no. DE-SC0008418 (DOE Early Career Program). We thank Mr. Anurag Kumar for helpful technical discussions.

References

1 J. S. Lee, S. Locatelli, S. T. Oyama and M. Boudart, *J. Catal.*, 1990, **125**, 157–170.

2 G. S. Ranhotra, A. T. Bell and J. A. Reimer, *J. Catal.*, 1987, **108**, 40–49.

3 C. Liu, M. Lin, K. Fang, Y. Meng and Y. Sun, *RSC Adv.*, 2014, **4**, 20948–20954.

4 H. Shou and R. J. Davis, *J. Catal.*, 2013, **306**, 91–99.

5 J. A. Schaidle and L. T. Thompson, *J. Catal.*, 2015, **329**, 325–334.

6 Y. Aoki, H. Tominaga and M. Nagai, *Catal. Today*, 2013, **215**, 169–175.

7 J.-S. Choi, G. Bugli and G. Djéga-Mariadassou, *J. Catal.*, 2000, **193**, 238–247.

8 G. S. Ranhotra, G. W. Haddix, A. T. Bell and J. A. Reimer, *J. Catal.*, 1987, **108**, 24–39.

9 C. Pham-Huu, M. J. Ledoux and J. Guille, *J. Catal.*, 1993, **143**, 249–261.

10 F. H. Ribeiro, M. Boudart, R. A. Dalla Betta and E. Iglesia, *J. Catal.*, 1991, **513**, 498–513.

11 E. Iglesia, J. E. Baumgartner, F. H. Ribeiro and M. Boudart, *J. Catal.*, 1991, **131**, 523–544.

12 F. H. Ribeiro, R. A. Dalla Betta, M. Boudart, J. Baumgartner and E. Iglesia, *J. Catal.*, 1991, **130**, 86–105.

13 P. C. K. Vesborg, B. Seger and I. Chorkendorff, *J. Phys. Chem. Lett.*, 2015, **6**, 951–957.

14 B. Sljukic, M. Vujkovic, L. Amaral, D. M. F. Santos, R. P. Rocha, C. A. C. Sequeira and J. L. Figueiredo, *J. Mater. Chem. A*, 2015, **3**, 15505–15512.

15 S. T. Hunt, T. Nimmanwudipong and Y. Román-Leshkov, *Angew. Chemie Int. Ed.*, 2014, **53**, 5131–5136.

16 S. K. Bej and L. T. Thompson, *Appl. Catal. A Gen.*, 2004, **264**, 141–150.

17 K. Xiong, W. Yu, D. G. Vlachos and J. G. Chen, *ChemCatChem*, 2015, **7**, 1402–1421.

18 K. Xiong, W. Yu and J. G. Chen, *Appl. Surf. Sci.*, 2014, **323**, 88–95.

19 H. Ren, W. Yu, M. Salciccioli, Y. Chen, Y. Huang, K. Xiong, D. G. Vlachos and J. G. Chen, *ChemSusChem*, 2013, **6**, 798–801.

20 J. Han, J. Duan, P. Chen, H. Lou, X. Zheng and H. Hong, *ChemSusChem*, 2012, **5**, 727–733.

21 J. Han, J. Duan, P. Chen, H. Lou, X. Zheng and H. Hong, *Green Chem.*, 2011, **13**, 2561.

22 S. A. W. Hollak, R. W. Gosselink, D. S. van Es and J. H. Bitter, *ACS Catal.*, 2013, **3**, 2837–2844.

23 R. W. Gosselink, D. R. Stellwagen and J. H. Bitter, *Angew. Chem. Int. Ed.*, 2013, **52**, 5089–5092.

24 A. L. Jongerius, R. W. Gosselink, J. Dijkstra, J. H. Bitter, P. C. A. Bruijnincx and B. M. Weckhuysen, *ChemCatChem*, 2013, **5**, 2964–2972.

25 T. Prasomsri, M. Shetty, K. Murugappan and Y. Roman-Leshkov, *Energy Environ. Sci.*, 2014, **7**, 2660–2669.

26 S. Boullosa-Eiras, R. Lødeng, H. Bergem, M. Stöcker, L. Hannevold and E. A. Blekkan, *Catal. Today*, 2014, **223**, 44–53.

27 S. T. Oyama, *The chemistry of transition metal carbides and nitrides*, London : Blackie Academic, 1996.

28 E. I. Ko and R. J. Madix, *Surf. Sci.*, 1981, **109**, 221–238.

29 A. L. Stottlemyer, T. G. Kelly, Q. Meng and J. G. Chen, *Surf. Sci. Rep.*, 2012, **67**, 201–232.

30 X.-R. Shi, S.-G. Wang, J. Hu, Z. Qin and J. Wang, *Surf. Sci.*, 2012, **606**, 1187–1194.

31 T. Wang, S. Wang, Y.-W. Li, J. Wang and H. Jiao, *J. Phys. Chem. C*, 2012, **116**, 6340–6348.

32 T. Wang, Y. W. Li, J. G. Wang, M. Beller and H. J. Jiao, *J. Phys. Chem. C*, 2014, **118**, 3162–3171.

33 T. Wang, Y.-W. Li, J. Wang, M. Beller and H. Jiao, *J. Phys. Chem. C*, 2014, **118**, 8079–8089.

34 T. Wang, Q. Luo, Y.-W. W. Li, J. Wang, M. Beller and H. Jiao, *Appl. Catal. A Gen.*, 2014, **478**, 146–156.

35 K. J. Leary, J. N. Michaels and M. Stacy, *J. Catal.*, 1986, **101**, 301–313.

36 E. Furimsky, *Appl. Catal. A Gen.*, 2000, **199**, 147–190.

37 C. Zhao, Y. Kou, A. A. Lemonidou, X. Li and J. A. Lercher, *Angew. Chem. Int. Ed.*, 2009, **48**, 3987–3990.

38 M. Saidi, F. Samimi, D. Karimipourfard, T. Nimmanwudipong, B. C. Gates and M. R. Rahimpour, *Energy Environ. Sci.*, 2014, **7**, 103–129.

39 H. Wang, J. Male and Y. Wang, *ACS Catal.*, 2013, **3**, 1047–1070.

40 J.-S. Choi, G. Bugli and G. Djéga-Mariadassou, in *12th International Congress on Catalysis: Proceedings of the 12th ICC, Granada, Spain, July 9-14, 2000*, eds. A. Corma, F. V. Melo, S. Mendioroz and J. L. G. Fierro, Elsevier, 2000, vol. 130, pp. 2885–2890.

41 S. T. Oyama, *Catal. Today*, 1992, **15**, 179–200.

42 D. Oliveira, D. R. Salahub, H. A. De Abreu and A. Duarte, *J. Phys. Chem. C*, 2014, **118**, 25517–25524.

43 J. S. Lee, L. Volpe, F. H. Ribeiro and M. Boudart, *J. Catal.*, 1988, **112**, 44–53.

44 E. Parthé and V. Sadogopan, *Acta Crystallogr.*, 1963, **16**, 202–205.

45 C. Bouchy, C. Pham-Huu, B. Heinrich, C. Chaumont and M. J. Ledoux, *J. Catal.*, 2000, **190**, 92–103.

46 R. R. Oliveira, A. S. Rocha, V. T. da Silva and A. B. Rocha, *Appl. Catal. A Gen.*, 2014, **469**, 139–145.

47 J. H. Sinfelt and D. J. C. Yates, *Nat. Phys. Sci.*, 1971, **229**, 27–28.

48 J. G. Chen, *Chem. Rev.*, 1996, **96**, 1477–1498.

49 J. S. Lee, S. T. Oyama and M. Boudart, *J. Catal.*, 1987, **106**, 125–133.

50 E. I. Ko and R. J. Madix, *Surf. Sci. Lett.*, 1980, **100**, L449–L453.

51 B. Frühberger and J. G. Chen, *J. Am. Chem. Soc.*, 1996, **118**, 11599–11609.

52 T. G. Kelly and J. G. Chen, *Green Chem.*, 2014, **16**, 777.

53 H. Ren, Y. Chen, Y. Huang, W. Deng, D. G. Vlachos and J. G. Chen, *Green Chem.*, 2014, **16**, 761–769.

54 M. K. Neylon, S. Choi, H. Kwon, K. E. Curry and L. T. Thompson, *Appl. Catal. A Gen.*, 1999, **183**, 253–263.

55 M. J. Ledoux, C. Pham-Huu, J. Guille and H. Dunlop, *J. Catal.*, 1992, **134**, 383–398.

56 K.-Z. Qi, G.-C. Wang and W.-J. Zheng, *Appl. Surf. Sci.*, 2013, **276**, 369–376.

57 B. Frank, T. P. Cotter, M. E. Schuster, R. Schlögl and A. Trunschke, *Chem. Eur. J.*, 2013, **19**, 16938–16945.

58 K.-Z. Qi, G.-C. Wang and W.-J. Zheng, *Surf. Sci.*, 2013, **614**, 53–63.

59 S. Posada-Pérez, F. Viñes, P. J. Ramirez, A. B. Vidal, J. A. Rodriguez and F. Illas, *Phys. Chem. Chem. Phys.*, 2014, **16**, 14912–14921.

60 M. D. Porosoff, X. Yang, J. A. Boscoboinik and J. G. Chen, *Angew. Chemie Int. Ed.*, 2014, **53**, 6705–6709.

61 Y. Choi, J. Lee, J. Shin, S. Lee, D. Kim and J. K. Lee, *Appl. Catal. A Gen.*, 2015, **492**, 140–150.

62 M.-L. Frauwallner, F. López-Linares, J. Lara-Romero, C. E. Scott, V. Ali, E. Hernández and P. Pereira-Almao, *Appl. Catal. A Gen.*, 2011, **394**, 62–70.

63 J. S. Lee, M. H. Yeom, K. Y. Y. Park, I.-S. Nam, J. S. Chung, Y. G. Kim and S. H. Moon, *J. Catal.*, 1991, **128**, 126–136.

64 J.-S. Choi, J. M. Krafft, A. Krzton and G. Djéga-Mariadassou, *Catal. Lett.*, 2002, **81**, 175–180.

65 S. J. Ardakani, X. Liu and K. J. Smith, *Appl. Catal. A Gen.*, 2007, **324**, 9–19.

66 W.-S. Lee, Z. Wang, R. J. Wu and A. Bhan, *J. Catal.*, 2014, **319**, 44–53.

67 A. F. Lamic, T. L. H. Pham, C. Potvin, J. M. Manoli and G. Djéga-Mariadassou, *J. Mol. Catal. A Chem.*, 2005, **237**, 109–114.

68 M. M. Sullivan, J. T. Held and A. Bhan, *J. Catal.*, 2015, **326**, 82–91.

69 D. A. Ruddy, J. A. Schaidle, J. R. Ferrell III, J. Wang, L. Moens and J. E. Hensley, *Green Chem.*, 2014, **16**, 454.

70 D. C. Elliott, *Energy Fuels*, 2007, **21**, 1792–1815.

71 Q. Bu, H. Lei, A. H. Zacher, L. Wang, S. Ren, J. Liang, Y. Wei, Y. Liu, J. Tang, Q. Zhang and R. Ruan, *Bioresour. Technol.*, 2012, **124**, 470–477.

72 T. V. Choudhary and C. B. Phillips, *Appl. Catal. A Gen.*, 2011, **397**, 1–12.

73 L. Zhang, R. Liu, R. Yin and Y. Mei, *Renew. Sustain. Energy Rev.*, 2013, **24**, 66–72.

74 M. Siaj, I. Temprano, N. Dubuc and P. H. McBreen, *J. Organomet. Chem.*, 2006, **691**, 5497–5504.

75 E. M. Zahidi, H. Oudghiri-Hassani and P. H. McBreen, *Nature*, 2001, **409**, 1023–1026.

76 K. Xiong, W. S. Lee, A. Bhan and J. G. Chen, *ChemSusChem*, 2014, **7**, 2146–2149.

77 W.-S. Lee, Z. Wang, W. Zheng, D. G. Vlachos and A. Bhan, *Catal. Sci. Technol.*, 2014, **4**, 2340–2352.

78 C.-J. Chen, W.-S. Lee and A. Bhan, *Appl. Catal. A Gen.*, 2016, **510**, 42–48.

79 M. Shetty, K. Murugappan, T. Prasomsri, W. H. Green and Y. Román-Leshkov, *J. Catal.*, 2015, **331**, 86–97.

80 E. Santillan-Jimenez, M. Perdu, R. Pace, T. Morgan and M. Crocker, *Catalysts*, 2015, **5**, 424–441.

81 J. Chang, T. Danuthai, S. Dewiyanti, C. Wang and A. Borgna, *ChemCatChem*, 2013, **5**, 3041–3049.

82 V. M. L. Whiffen and K. J. Smith, *Energy Fuels*, 2010, **24**, 4728–4737.

83 P. M. Mortensen, J.-D. Grunwaldt, P. A. Jensen and A. D. Jensen, *ACS Catal.*, 2013, **3**, 1774–1785.

84 P. M. Mortensen, H. W. P. de Carvalho, J.-D. Grunwaldt, P. A. Jensen and A. D. Jensen, *J. Catal.*, 2015, **328**, 208–215.

85 D. R. Stellwagen and J. H. Bitter, *Green Chem.*, 2015, **17**, 582–593.

86 J. Han, J. Duan, P. Chen, H. Lou and X. Zheng, *Adv. Synth. Catal.*, 2011, **353**, 2577–2583.

87 M. Lu, F. Lu, J. Zhu, M. Li, J. Zhu and Y. Shan, *React. Kinet. Mech. Catal.*, 2015, **115**, 251–262.

88 E. F. Mai, M. A. Machado, T. E. Davies, J. A. Lopez-Sanchez and V. T. da Silva, *Green Chem.*, 2014, **16**, 4092–4097.

89 Y. Qin, L. He, J. Duan, P. Chen, H. Lou, X. Zheng and H. Hong, *ChemCatChem*, 2014, **6**, 2698–2705.

90 T. Matsuda, T. Ohno, H. Sakagami and N. Takahashi, *J. Jpn. Pet. Inst.*, 2007, **50**, 229–239.

91 T. Matsuda, H. Sakagami and N. Takahashi, *Appl. Catal. A Gen.*, 2001, **213**, 83–90.

92 P. Liu and J. A. Rodriguez, *J. Phys. Chem. B*, 2006, **110**, 19418–19425.

93 A. J. Medford, A. Vojvodic, F. Studt, F. Abild-Pedersen and J. K. Nørskov, *J. Catal.*, 2012, **290**, 108–117.

94 H. Tominaga and M. Nagai, *J. Phys. Chem. B*, 2005, **109**, 20415–20423.

95 K. D. Sabnis, Y. Cui, M. C. Akatay, M. Shekhar, W.-S. Lee, J. T. Miller, W. N. Delgass and F. H. Ribeiro, *J. Catal.*, 2015, **331**, 162–171.

96 T. Namiki, S. Yamashita, H. Tominaga and M. Nagai, *Appl. Catal. A Gen.*, 2011, **398**, 155–160.

97 J. Patt, D. J. Moon, C. Phillips and L. Thompson, *Catal. Letters*, 2000, **65**, 193–195.

98 J. D. Moon and J. W. Ryu, *Catal. Letters*, 2004, **92**, 2–9.

99 J.-S. Choi, V. Schwartz, E. Santillan-Jimenez, M. Crocker, S. Lewis, M. Lance, H. Meyer and K. More, *Catalysts*, 2015, **5**, 406–423.

100 V. Keller, P. Wehrer, F. Garin, R. Ducros and G. Maire, *J. Catal.*, 1997, **166**, 125–135.

101 A. F. Lamic, C. H. Shin, G. Djéga-Mariadassou and C. Potvin, *Appl. Catal. A Gen.*, 2006, **302**, 5–13.

102 N. Ji, T. Zhang, M. Zheng, A. Wang, H. Wang, X. Wang, Y. Shu, A. L. Stottlemyer and J. G. Chen, *Catal. Today*, 2009, **147**, 77–85.

103 C. D. Baertsch, K. T. Komala, Y.-H. Chua and E. Iglesia, *J. Catal.*, 2002, **205**, 44–57.

104 V. Keller, F. Wehrer, F. Garin, R. Ducros and G. Maire, *J. Catal.*, 1995, **153**, 9–16.

105 F. Garin, V. Keller, R. Ducros, A. Muller and G. Maire, *J. Catal.*, 1997, **166**, 136–147.

106 L. Leclercq, M. Provost, H. Pastor and G. Leclercq, *J. Catal.*, 1989, **117**, 384–395.

107 D. A. Gómez-Gualdrón and P. B. Balbuena, *Nanotechnology*, 2009, **20**, 215601.

108 G. E. Ramírez-Caballero, J. C. Burgos and P. B. Balbuena, *J. Phys. Chem. C*, 2009, **113**, 15658–15666.

109 W.-S. Lee, A. Kumar, Z. Wang and A. Bhan, *ACS Catal.*, 2015, **5**, 4104–4114.

110 M. Chia, Y. J. Pagán-Torres, D. Hibbitts, Q. Tan, H. N. Pham, A. K. Datye, M. Neurock, R. J. Davis and J. A. Dumesic, *J. Am. Chem. Soc.*, 2011, **133**, 12675–12689.